Journal of ELECTRONIC MATERIALS, Vol. 42, No. 6, 2013
DOI: 10.1007/s11664-013-2515-1
© 2013 TMS

Effect of Applied Load in the Nanoindentation of Gold Ball Bonds

MUHAMMAD NUBLI ZULKIFLI,[1] AZMAN JALAR,[1,4] SHAHRUM ABDULLAH,[2] IRMAN ABDUL RAHMAN,[3] and NORINSAN KAMIL OTHMAN[3]

1.—Institute of Microengineering and Nanoelectronics (IMEN), Universiti Kebangsaan Malaysia, 43600 UKM Bangi, Selangor, Malaysia. 2.—Department of Mechanical & Materials Engineering, Universiti Kebangsaan Malaysia, 43600 UKM Bangi, Selangor, Malaysia. 3.—School of Applied Physics, Faculty of Science and Technology, Universiti Kebangsaan Malaysia, 43600 UKM Bangi, Selangor, Malaysia. 4.—e-mail: azmn@ukm.my

We have analyzed the effects of nanoindentation at applied loads of 10 mN and 20 mN on the micromechanical properties of gold (Au) ball bonds with and without cracks. The depth profile and the plastic zone size for each indentation were determined to identify the substrate effect and its relationship with the observed micromechanical properties. The substrate effect occurred for indentations at 20 mN applied load, but did not occur near cracks for either 10 mN or 20 mN loads. Because of the substrate effect and the presence of cracks, the average hardness or yield strength decreased for indentations on Au ball bonds. Therefore, to minimize the substrate effect, an applied load of 10 mN is best for characterizing Au ball bonds.

Key words: Nanoindentation, Au ball bond, bonding ability, applied load, substrate effect

INTRODUCTION

Because of its technological maturity and cost effectiveness, wire bonding is still the most preferred interconnection technique for electronics packaging despite the introduction of other methods such as flip-chip attachment and tape-automated bonding.[1–5] To decrease the form factor in shrinking electronics packages, the bond pad pitch and the ball bond size need to become ever smaller. Consequently, this will introduce measurement challenges in evaluating the bondability and reliability of ball bonds.

Conventional tests for evaluating the quality of ball bonds such as wire pulling and ball shearing have also become problematic.[2,4–11] Sundaraman et al.[6] found that stresses induced in the silicon substrate under the bond pad are sensitive to the angle of the wire pull; the lowest stresses are produced by pulls normal to the bond pad surface. The stress distribution is also affected by the angle of the pull, where higher angles produce higher stress values. The elongation of the wire also affects wire pull tests.[7,8] Wires with a larger percentage elongation have larger bond pull strengths because of the increase in the final loop height at wire breakage. The bond pull strength is also a function of the wire loop geometry.[8] It has been observed that, when the difference in height between the first and second bonds decreases, the bond pull strength decreases. Harman[2] found that the position of the hook and the pull angle have a significant effect on the wire pull results, owing to the different distribution of forces on the wire bond. The bond pad also has a tendency to peel off when the position of the hook is moved close to the wedge bond.[2,7] In addition, the variability of the results for wire pulls increases and the average value of the bond pull force becomes lower, when the hook is placed near the wedge bond.[2] The pull strength of the wire bond also depends on the character of the bond. During the wire pull test the ball bond remains untested because the weak area is located at the wire and not

(Received July 15, 2012; accepted January 21, 2013; published online March 5, 2013)

at the ball bond.[8] The measurement of the ball bond contact area becomes more difficult for finer-pitch ball bonds,[2,9,10] since it is hidden when the ball bond is viewed in a vertical perspective with an optical microscope. The shear tool drag for ball shearing becomes a more critical problem for finer-pitch ball bonds because of the difficulty in the vertical positioning of the tool.[2] Furthermore, void creation within ball bonds caused by degradation during high-temperature storage is not observed in the ball bond shear test.[11]

In the present analysis, the nanoindentation approach is used to characterize the performance of gold (Au) ball bonds in a more detailed and localized manner. Several researchers have used nanoindentation to characterize the micromechanical properties of wire bonds.[12–15] Saraswati et al.[12] carried out nanoindentation on calcium-doped wire bonds using a cyclic load–partial unload technique. It was found that calcium at 1 ppm levels influences the cyclic load–depth curve. Shah et al.[13] analyzed the factors influencing the loop height of wire bonds by using nanoindentation and observed that the hardness at the heat-affected zone has a V-shaped profile. Agyakwa et al.[14] characterized the micromechanical properties of Al wedge bonds at bond interfaces that have undergone various thermal cycles and found that a wire bond subjected to a junction temperature cycle of −55°C to −125°C was harder than one cycled at −60°C to 170°C. Jalar et al.[15] carried out nanoindentation tests to measure the hardness of the Au base metal and the intermetallic compound (IMC) composing the Au ball bond; the IMC has a higher value of hardness and a greater tendency for brittle fracture relative to the Au base metal.

Most of the nanoindentation studies on wire bonds used a single applied load to create a specific indentation depth.[12–15] Since the effects of various applied loads on Au ball bonds have not been studied in detail, further analysis is required. Thus, the effect of applied load (specifically, 10 mN and 20 mN) on Au ball bond nanoindentation was analyzed here by performing cyclic load–partial unload tests. Changes in volume or indentation depth, plastic zone size, and micromechanical properties were used to evaluate the effects of 10 mN and 20 mN applied loads and to determine which load is optimum for these measurements.

EXPERIMENTAL PROCEDURES

The samples were Au ball bonds at aluminum (Al) bond pads of quad-flat no-leads (QFN) packages that were prepared for nanoindentation by resin mounting. The selected QFN packages were built by the Advanced Semiconductor Packaging (ASPAC) research group of Universiti Kebangsaan Malaysia (UKM). Two types of Au ball bonds were examined from the as-fabricated QFN packages: with optimized and nonoptimized wire-bonding parameters. The four parameters were bonding power, bonding time, bonding force, and stage temperature. In addition, cracks may be present at the periphery of Au ball bonds from the QFN having nonoptimized wire-bonding parameters; they are not present in the QFN having optimized wire-bonding parameters. To expose a Au ball bond in the QFN package after mounting and curing, wet grinding was performed with 600, 800, and 1200 grit abrasive paper, followed by polishing with 6 μm, 3 μm, 1 μm, and 0.25 μm diamond suspensions on silk cloths.

Nanoindentation tests were performed with a Micro Materials Nanotest™ indenter equipped with a Berkovich diamond tip. Four indentations were made on each sample. The distance between the Au and the Al IMC was maintained at 6 μm, and the indentation spacing was maintained at 12 μm. Ten cycles of load–partial unload tests with maximum depth of 1500 nm and maximum load of 50 mN were performed to analyze the effect of applied load (10 mN versus 20 mN) and depth on the Au ball bonds. Table I summarizes the experiments that were carried out.

Nanoindentation was performed at room temperature with loading and unloading rates of 0.5 mN/s, with 10 s hold time at the peak load to account for creep and 60 s hold time at 90% unloading for thermal drift correction. The experiments and subsequent analyses were based on the Oliver and Pharr method,[16] which determines the hardness and the reduced Young's modulus from depth-sensing indentation, load–displacement data. The hardness H is given as:[16]

$$H = \frac{P_{\max}}{A}, \quad (1)$$

where $P_{\max}$ is the maximum load and A is the projected area of contact. The reduced modulus is:[16,17]

Table I. Experiments to analyze the effect of applied load on Au ball bonds from as-fabricated QFN with optimized and nonoptimized wire-bonding parameter

Experiment	Au Ball Bond Condition	Load (mN)
1	Optimized	10
2	Optimized	20
3	Nonoptimized	10
4	Nonoptimized	20

$$E_r = \frac{\sqrt{\pi}}{\sqrt{A_c}} S, \quad (2)$$

where S is the contact stiffness corresponding to the slope of the load–depth curve at the beginning of unloading, and A_c is the contact area. E_r is also given by Ref. 16 as

$$\frac{1}{E_r} = \frac{1-\upsilon_i^2}{E_i} + \frac{1-\upsilon_s^2}{E_s}, \quad (3)$$

where υ_i and E_i are the Poisson's ratio and Young's modulus of the indenter, respectively, and υ_s and E_s are the corresponding values of the sample. The diamond indenter tip has a Poisson's ratio of 0.07 and Young's modulus of 1140 GPa.

After the nanoindentation tests, optical images were acquired with an Alicona™ infinite-focus microscope (IFM) to measure the depth profiles of the indentations on the Au ball bonds and to analyze the physical behavior or volume changes of the imprinted indentations.

RESULTS AND DISCUSSION

Figure 1 shows the location of indentations that have been made on the cross-sectioned Au ball bond from the cyclic load–partial unload tests, while Fig. 2 shows the corresponding load–depth (P–h) profiles for each test.

In Fig. 2, the increments of applied load and plastic depth for each cycle are 5 mN and 150 nm, respectively. The profiles of the P–h curves in Fig. 2 indicate early signs of variation, especially in final indentation depth,[16] for each indentation made during the cyclic load–partial unload tests. According to the Oliver and Pharr method,[16] the variation of the final indentation depth affects the values of the hardness and reduced modulus. Thus, two types of profiles, namely hardness versus plastic depth and reduced modulus versus plastic depth, were created to analyze in more detail the changes in micromechanical properties of the Au ball bonds with regard to applied load and indentation depth. Figure 3 displays these profiles.

In Fig. 3a, it is noted that the hardness of each of the indentations across the Au ball bond starts at a high value and gradually decreases after the plastic depth reaches more than 400 nm. Based on Fig. 2, the applied load is approximately 8 mN at this plastic depth. The higher value of hardness at the lower depth is due to the strain hardening effect and the indentation size effect (ISE).[18–26] The strain hardening effect occurs when the Au ball bond experiences deformation during the wire-bonding process;[18,19] it may also originate from the mechanical grinding and polishing processes.[20,21] The ISE is due to nucleation of dislocations within the plastic zone of the sample.[22–26] Nix and Gao[22] reported that the ISE derives from a strain gradient, and they also noted that decreased indentation depth reduces the geometrically necessary dislocation density and effectively increases the hardness of the sample.[22] Therefore, to avoid the strain hardening and indentation size effects, applied loads larger than 10 mN that produce indentation depths greater than 400 nm were used for the subsequent analyses. In contrast, Fig. 3b shows that the reduced modulus versus plastic depth profiles exhibit different trends, especially in terms of the initial reduced modulus for each indentation, relative to the hardness versus plastic depth profiles. Indentations 1, 2, and 4 have higher initial reduced moduli, while indentation 3 has a lower value. The peak of reduced modulus at 300 nm plastic depth can be seen for indentation 3 only. The reduced modulus of metals is due to the intrinsic behavior, rather than physical changes of indention depth or plastic depth.[13,27] Thus, the inconsistent trend of reduced modulus versus depth is an intrinsic behavior of Au.

Figure 4 shows the location of indentations made on Au ball bonds on QFN samples with optimized and nonoptimized wire-bonding parameters; also shown are the 6-μm separations between indentations near the IMC or crack. Each of the indentations in Fig. 4 is

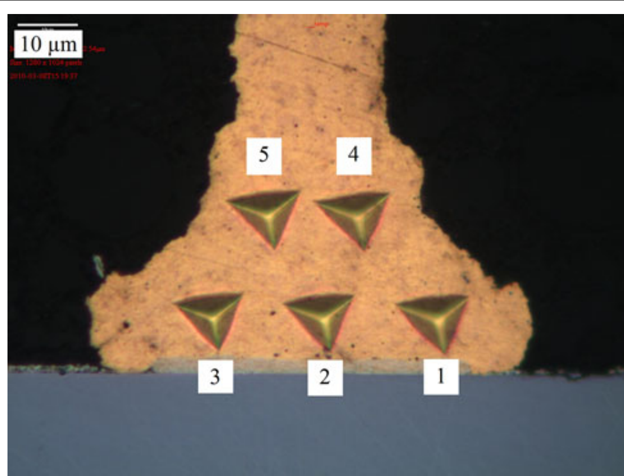

Fig. 1. Location of indentations on a Au ball bond from a cyclic load–partial unload test.

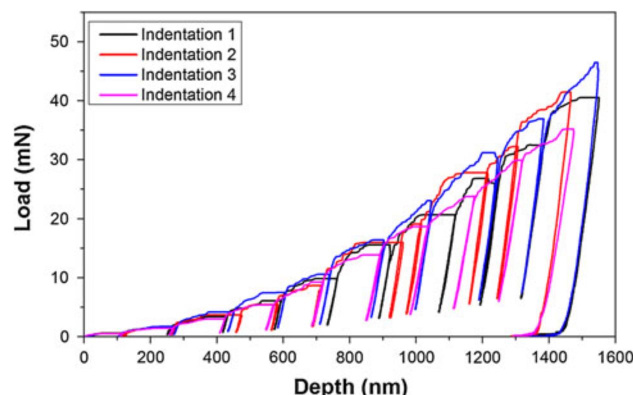

Fig. 2. P–h profile for a cyclic load–partial unload test.

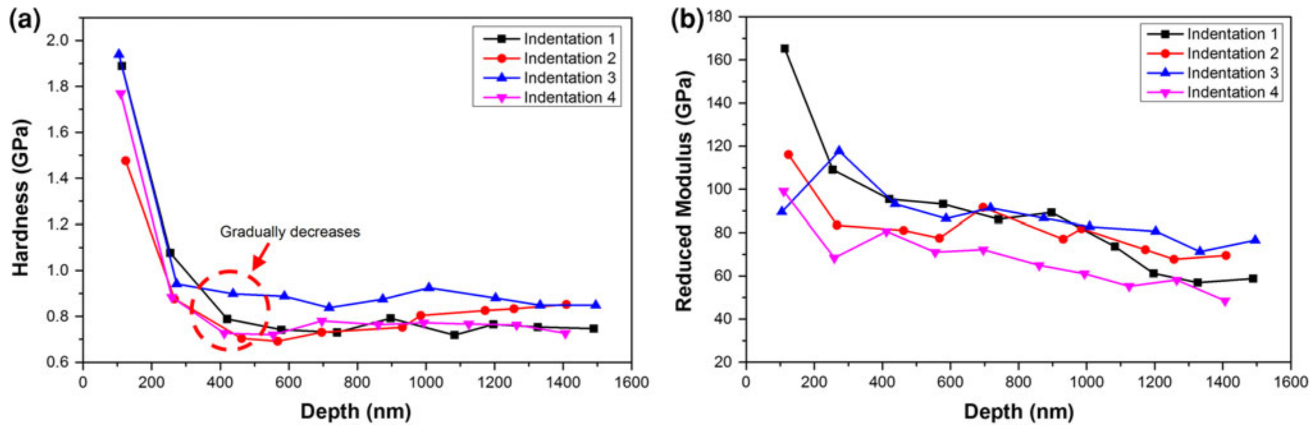

Fig. 3. Profiles of (a) hardness versus plastic depth and (b) reduced modulus versus plastic depth.

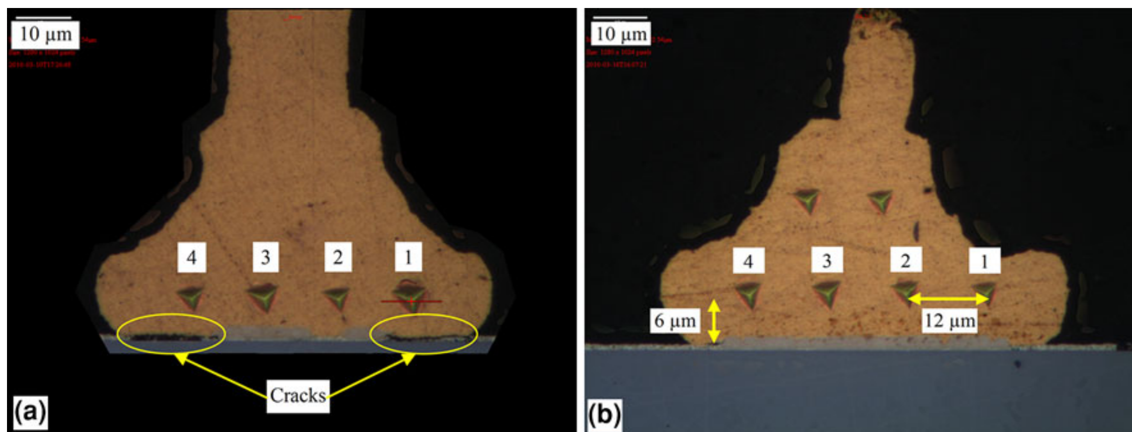

Fig. 4. Indentation locations for Au ball bonds (a) with crack and (b) without crack.

assigned a number (1 to 4). Figure 5 exhibits the *P–h* profiles for indentations made during the experiments listed in Table I.

In Fig. 5, the *P–h* profile for each indentation has a different shape based on the applied load and the location of the indentation. *P–h* profiles for the indentations from experiments 1 and 2 (Table I) have typical shapes (Fig. 5a, b) that have less variation in the final indentation depth and compliance. In contrast, the *P–h* profiles for experiments 3 and 4 have distinct changes in the final indentation depth and compliance (Fig. 5c, d). The Au ball bonds in experiments 1 and 2 do not have cracks, whereas in experiments 3 and 4 they do. One can identify increased compliance in a *P–h* profile by a less steep loading curve and a deeper indentation.[28–30] The *P–h* profiles for indentation 2 from experiments 1 to 4 were selected to compare the compliances of the Au ball bonds. Figure 6a depicts data from experiments 1 and 3 that had an applied load of 10 mN, while Fig. 6b depicts data from experiments 2 and 4 that had an applied load of 20 mN.

In Fig. 6a it is seen that, when a 10 mN load is applied, the *P–h* profile for indentation 2 in the Au ball bond with cracks (experiment 3) possesses a less steep loading curve and a higher indentation depth relative to that of a Au ball bond without a crack (experiment 1). Similarly, for the 20 mN applied load, the *P–h* profile for indentation 2 from the Au ball bond with cracks (experiment 2) possesses a less steep lower loading curve and a higher indentation depth relative to that of a Au ball bond without a crack (experiment 4). The similar behavior for different applied loads indicates that the increased compliance is due to the presence of cracks in the Au ball bond sample. The presence of cracks effectively decreases the sample boundary. Several studies have indicated that a decrease in the sample boundary will increase the compliance in a *P–h* profile.[28,29,31] Choi and Suresh[29] reported that the existence of a free surface at the sample boundary results in decreased yield strength and deformation during nanoindentation. Lian et al.[31] simulated nanoindentation using molecular dynamics and found that a decrease in the sample boundary will annihilate the dislocation created from the plastic deformation during nanoindentation.

In Fig. 5d it can be seen that the *P–h* profile for indentation 4 from experiment 4 differs from other

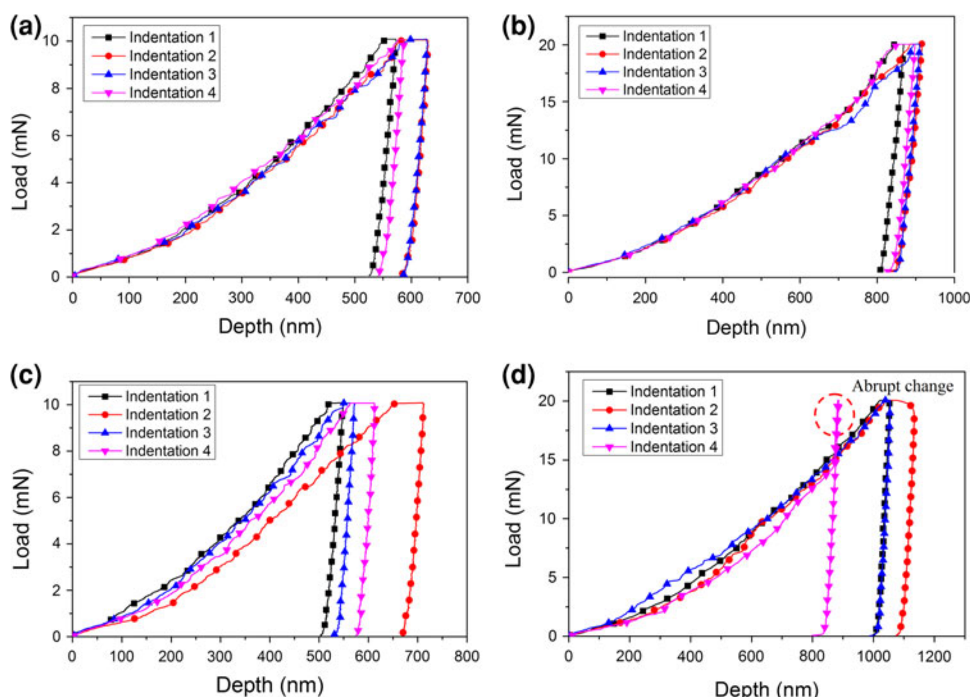

Fig. 5. *P–h* profiles for indentations from (a) experiment 1, (b) experiment 2, (c) experiment 3, and (d) experiment 4.

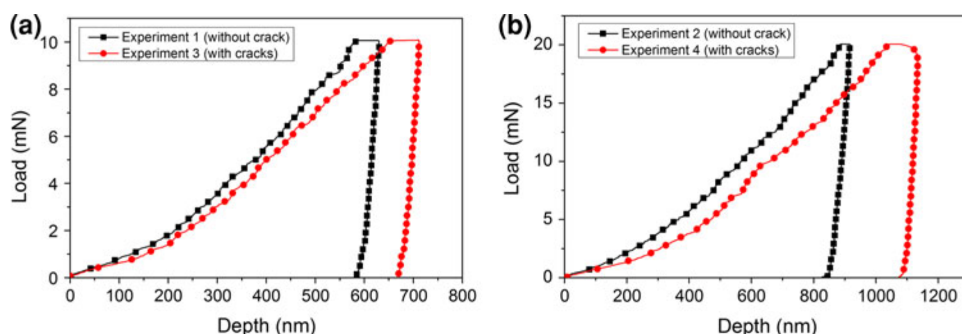

Fig. 6. *P–h* profiles for indentation 2 from (a) experiments 1 and 3 with applied load of 10 mN, and (b) experiments 2 and 4 with applied load of 20 mN.

indentations because it has an abrupt change at the maximum load and a small indentation depth gradient. Wang et al.[32] and Daugela et al.[33] reported similar behavior. Wang et al.[32] conducted nanoindentation tests on a composite material strengthened by fiber steel and observed that an abrupt change in the *P–h* profile indicates the presence of cracks and voids near the indentation. Similarly, Daugela et al.[33] attributed an abrupt change in the nanoindentation *P–h* profile of a low-*k* dielectric material to the presence of cracks or voids. According to the expanding cavity model, an abrupt change in a *P–h* profile may indicate that the propagation of the plastic zone has reached a crack.[28]

Figure 7a depicts a three-dimensional (3D) image constructed from IFM data. Figure 7b shows a schematic illustration of pile-up and substrate effects in a cross-sectional view of indentation.

The 3D image indicates that there are two types of physical change that can affect the nanoindentation results, i.e., pile-up and the substrate effect, which can result in either underestimation or overestimation of the nanoindentation results.[17] Pile-up and substrate effects occur because of plastic deformation and can be noted by changes in the indentation contact area as shown in Fig. 7a–c. Pile-up usually happens in a material that is work-hardened prior to nanoindentation.[34,35] In the present case, mechanical grinding and polishing processes, as well as deformation phenomena from the wire-bonding process, are possible ways to work-harden the Au ball bond. However, the indentation that has pile-up, or “sinking-in,” still yields acceptable results.[17] (According to the ISO 14577 standard, the measurement of the micromechanical value for a

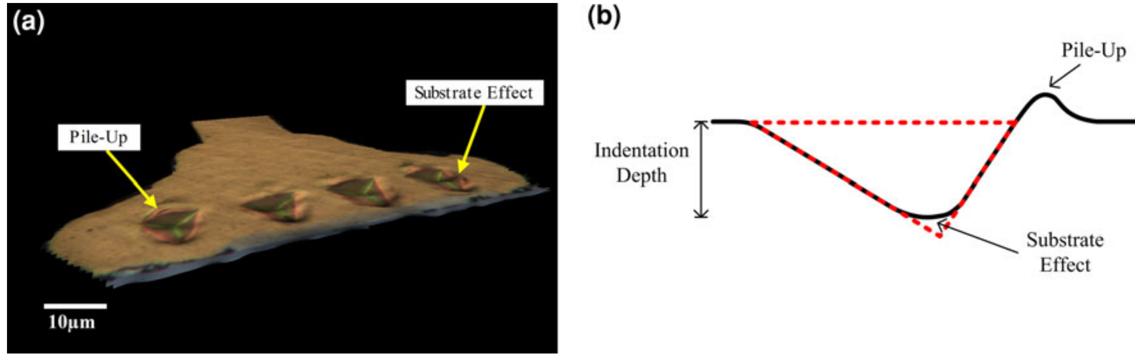

Fig. 7. (a) 3D image constructed from IFM images, and (b) schematic illustration of pile-up and substrate effects in cross-sectional view of indentation; the red dotted line is the cross-sectional view of the Berkovich indenter.

sample that exhibits pile-up is still acceptable for the purpose of comparison[17]). Oliver and Pharr[16] discussed the sinking-in effect in their analysis of hardness and reduced modulus. The substrate effect occurs because the plastic zone of the radial expansion cannot propagate to a wider volume because of blocking by harder materials (such as Au-Al IMC and silicon), and this results in the deviation of the valley region of the depth profile.[17] Therefore, the physical changes of the substrate effect due to the differing 10 mN and 20 mN results have been analyzed with IFM. Figures 8, 9, 10, and 11 show the depth profile for each indentation from experiments 1, 2, 3, and 4, respectively.

In Figs. 9 and 11, some of the indentations exhibit a shape deviation in the valley region of the depth profile that indicates a substrate effect. Normally, this region has a sharp profile determined by the 50-nm to 150-nm tip radius of the indenter.[36] To analyze the deviations in this region, the path length at indention depth of 50 nm was measured for each indentation in experiments 1, 2, 3, and 4, as shown in Figs. 8, 9, 10, and 11, respectively. Table II presents the deviation value for each indentation from experiments 1 to 4.

An indentation with deviation of more than 150 nm (indicated by bold values in Table II) has been influenced by the substrate effect, since the deviation is more than the maximum 150 nm range of the indenter profile. Experiments 2 and 4 (both 20 mN loads) exhibit the substrate effect, whereas experiments 1 and 3 (both 10 mN loads) do not. Thus, the substrate effect is more pronounced for higher applied loads, as shown in Figs. 9 and 11. To further analyze the substrate effect, a measurement of the plastic zone size c, based on the expanding cavity model, was performed for each indentation according to Ref. 28:

$$c = \sqrt{\frac{3P}{2\pi\sigma_y}}, \tag{4}$$

where P is the load and σ_y is the yield strength. The relationship between yield strength and hardness H is based on Tabor's relation[17]

$$\sigma_y = H/C, \tag{5}$$

where C is a constraint factor that is equal to 3 for metals.[17] Choi and Suresh[28] reported that the value of the plastic zone size c may extend as much as five times beyond the measured continuum plastic zone, based on the expanding cavity model widely used to model changes of elastic to plastic behavior during nanoindentation.[17,37] Therefore, Eq. 4 can be expressed as follows:

$$c = 5\left(\sqrt{\frac{3PC}{2\pi H}}\right). \tag{6}$$

Table III presents the value of c calculated from Eq. 6 for each indentation from experiments 1 to 4.

For each indentation in experiments 1 and 3, c is smaller than or equal to the 6-μm distance between the indentations and the Au-Al IMC. In contrast, for most of the indentations from experiments 2 and 4, c is greater than this distance, except for indentation 2 from experiment 4. According to Eq. 6, an increase of P will increase c. This explains why most of the indentations at the 20 mN applied load (experiments 2 and 4) have larger c sizes.

To analyze the substrate effect in more detail, a comparison was performed between the deviations in the depth profile valley (Table II) versus the plastic zone size c for each indentation (Table III). The substrate effect did not occur for any of the indentations in experiments 1 and 3, because of the lower or equal value of c compared with the distance between the indentations and the Au-Al IMC, as calculated from Eq. 6. Thus, an indentation imprinted on a Au ball bond that has a smaller or equal value of c is not affected by the substrate effect. In contrast, indentations 2, 3, and 4 from experiment 2 and indentations 2 and 3 from experiment 4 exhibit the substrate effect. In addition, the

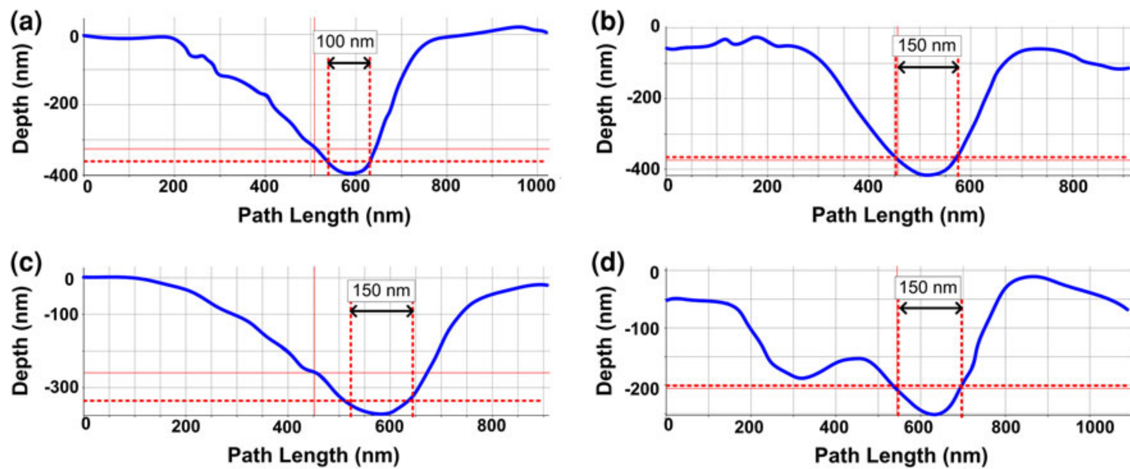

Fig. 8. Depth profile for each indentation from experiment 1: (a) indentation 1, (b) indentation 2, (c) indentation 3, and (d) indentation 4. Dotted lines indicate the path length at depth of 50 nm.

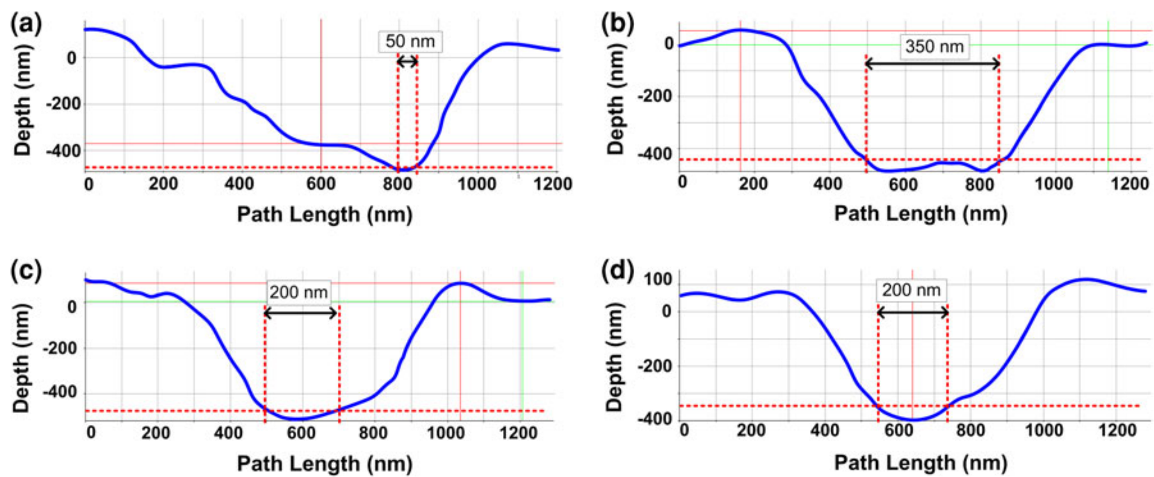

Fig. 9. Depth profile for each indentation from experiment 2: (a) indentation 1, (b) indentation 2, (c) indentation 3, and (d) indentation 4. Dotted lines indicate the path length at depth of 50 nm.

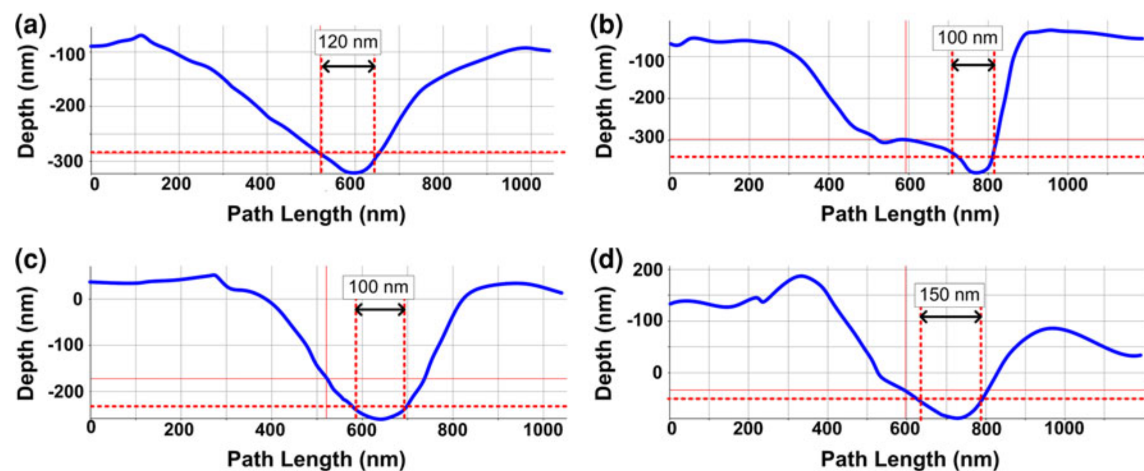

Fig. 10. Depth profile for each indentation from experiment 3: (a) indentation 1, (b) indentation 2, (c) indentation 3, and (d) indentation 4. Dotted lines indicate the path length at depth of 50 nm.

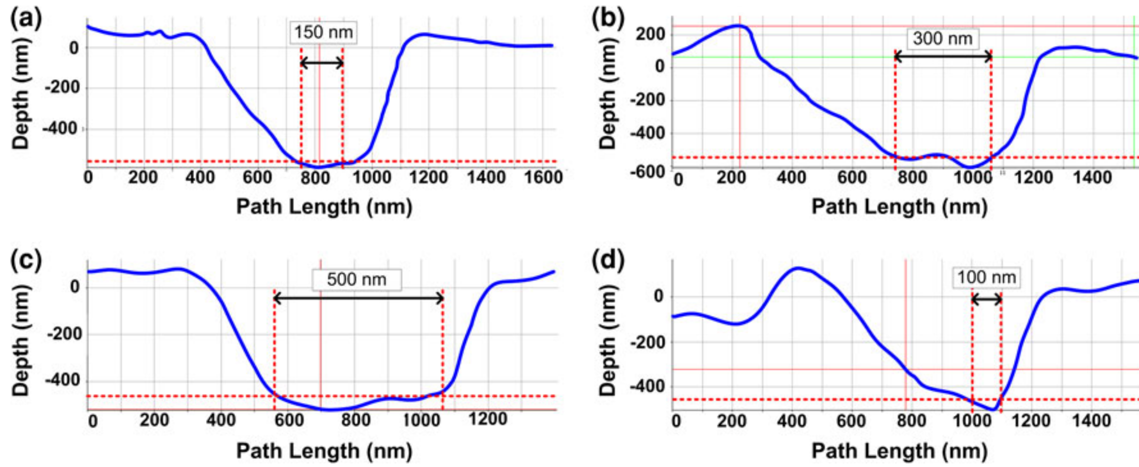

Fig. 11. Depth profile for each indentation from experiment 4: (a) indentation 1, (b) indentation 2, (c) indentation 3, and (d) indentation 4. Dotted lines indicate the path length at depth of 50 nm.

Table II. Deviation value for each indentation from experiments 1 to 4

	Deviation (nm)			
Experiment	**Indentation 1**	**Indentation 2**	**Indentation 3**	**Indentation 4**
1	100	150	150	150
2	50	**350**	**200**	**200**
3	120	100	100	150
4	150	**300**	**500**	100

Table III. Plastic zone size *c* for each indentation from experiments 1 to 3, and calculated from Eq. 6

	c (μm)			
Indentation	**Experiment 1**	**Experiment 2**	**Experiment 3**	**Experiment 4**
1	5.612	8.094	6.079	7.483
2	6.350	8.579	5.690	1.043
3	6.259	8.302	5.726	8.124
4	5.091	8.158	5.027	9.625

c values in Table III are more than 6 μm, except for indentation 2 of experiment 4. As mentioned earlier, the substrate effect occurs because the plastic zone of the radial expansion cannot propagate to a wider volume because of blocking by harder materials (Au-Al IMC and silicon). This will cause the plastically deformed Au to flow backward towards the valley region and cause it to widen by more than 150 nm, as shown in Figs. 9b–d and 11b, c.[17] In addition, the c value for indentation 4 from experiment 4 in Table III is 9.625 μm, which is the highest value of all the indentations. This further explains the occurrence of the abrupt change in the *P*–*h* profile of indentation 4 from experiment 4 in Fig. 5d, compared with that of indentation 1 from experiment 4 and indentations 1 and 4 from experiment 3.

However, there is no occurrence of the substrate effect in indentation 1 of experiment 3 or in indentations 1 and 4 of experiment 4, as indicated in Table II. From Fig. 1 it is noted that a crack is close to and perpendicular to indentations 1 and 4 from experiments 3 and 4. Since the existence of a crack will annihilate the dislocation created from the propagation of a plastic zone,[28,29,31] the valley in the depth profile for indentation 1 from experiment 3, as well as those for indentations 1 and 4 from experiment 4, will have a shape that follows that of the tip.

The changes in the *P*–*h* profiles, indentation depth profiles, and plastic zone sizes c are some of the factors that can affect the micromechanical properties, especially hardness.[16,17] Table IV presents hardness values for each indentation from experiments 1 to 4, and Fig. 12 shows the variation of hardness in these indentations.

Table IV. Hardness values for each indentation from experiments 1 to 4

Indentation	Hardness (GPa)			
	Experiment 1	Experiment 2	Experiment 3	Experiment 4
1	1.137	1.093	0.969	1.279
2	0.888	0.973	1.106	0.658
3	0.914	1.039	1.092	1.085
4	1.381	1.076	1.417	0.773
Average	1.080	1.045	1.146	0.949

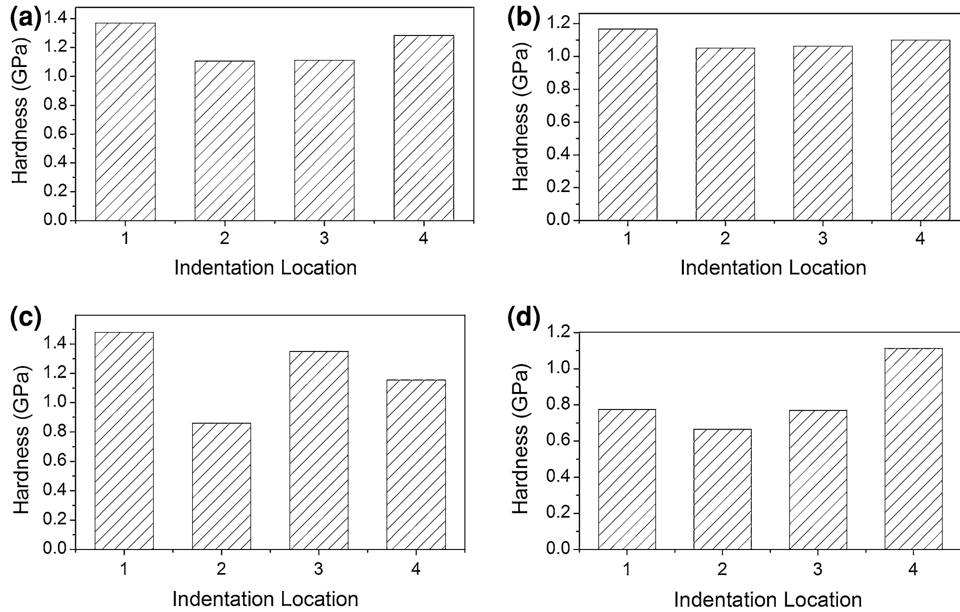

Fig. 12. Variation of hardness in indentations from: (a) experiment 1, (b) experiment 2, (c) experiment 3, and (d) experiment 4.

The indentations from experiment 4 have the lowest average hardness value (0.949 GPa), followed by that from indentations in experiment 2 (1.045 GPa). The substrate effect and the presence of a crack in experiment 4 may contribute to the low hardness or yield strength, as shown in Fig. 11 and indicated in Table II. However, the low hardness or yield strength in experiment 2 may be due solely to the substrate effect, as indicated in Fig. 9 and Table II. From Eq. 1, the projected area A has a different value as a result of the accumulation between the actual projected area produced by nanoindentation and the plastically deformed area caused by the substrate effect. If A is overestimated, then the hardness is reduced according to Eq. 1. Thus, to mitigate the substrate effect, 10 mN is better than 20 mN for characterizing Au ball bonds within the 6-μm distance between the indentation and the Au-Al IMC.

From Table IV and Fig. 12, it is shown that indentation 4 from experiment 4 has the lowest hardness value (0.773 GPa), followed by indentation 1 from experiment 3 (0.969 GPa). Both indentations were located close to and perpendicular to a crack, and these results are due to the reduction in yield strength or the annihilation of dislocations.[28,29,31] It is the actual value of hardness or yield strength that indicates the reduction in bondability of the Au ball bond for the indentations from experiments 2 and 4. This is because the projected areas A obtained for indention 4 from experiment 4 and for indentation 1 from experiment 3 have shapes that follow the profile of the indenter (Table II). Therefore, the increase in applied load from 10 mN in experiment 3 to 20 mN in experiment 4 does not affect the actual micromechanical properties of the indentations located near the cracks.

CONCLUSIONS

Nanoindentation has been conducted on Au ball bonds, with and without cracks. The effects of different applied loads (10 mN and 20 mN) were examined. Features in the P–h profile, such as an increase in compliance and the abrupt change at the maximum load with small indentation depth gradient, can be used to indicate the presence of cracks

in the Au ball bond sample. The substrate effect was apparent for indentations imprinted at 20 mN and not near a crack. In contrast, the 20 mN load does not affect the measurement of micromechanical properties for the indentations near a crack. For the indentations in experiment 4, the substrate effect and the presence of cracks contributed to the lowest average values of hardness or yield strength. Conversely, the second lowest average values of hardness or yield strength derived from the indentations in experiment 2 might be contributed solely by the substrate effect. This observation shows that the substrate effect significantly impacts the micromechanical properties obtained from nanoindentation. Thus, to minimize the substrate effect, a 10 mN applied load is more optimal for characterizing the Au ball bond, with a distance of 6 μm between the indentation and the Au-Al IMC.

ACKNOWLEDGEMENT

This work was sponsored by the Ministry of Higher Education of Malaysia under the Exploratory Research Grant Scheme (ERGS/1/2011/STG/UKM/02/10), OUP-2012-120, and UKM-RRR1-07-FRGS0257-2010.

REFERENCES

1. C.D. Breach and F.W. Wulff, *Microelectron. Reliab.* 50, 1 (2010).
2. G. Harman, *Wire Bonding in Microelectronics* (New York: McGraw-Hill, 2010), pp. 307–315.
3. R.R. Tummala, *Fundamentals of Microsystems Packaging* (New York: McGraw-Hill, 2001), pp. 311–312.
4. W.D.V. Driel, R.B.R.V. Silfhout, and G.Q. Zhang, *Microelectron. Int.* 25, 15 (2008).
5. Z.W. Zhong, *Microelectron. Int.* 26, 10 (2009).
6. V. Sundaraman, D.R. Edwards, W.E. Subido, and H.R. Test, *50th Electronic Components and Technology Conf.* (IEEE, Las Vegas, 2000), pp. 416–420.
7. G.G. Harman and C.A. Cannon, *IEEE Trans. Compon. Hybrids Manuf. Technol.* 3, 203 (1978).
8. M. Petch, D. Barker, and P. Lall, *IEEE Trans. Compon. Packag. Aging Manuf. Technol.* 17, 610 (1994).
9. Z.N. Liang, F.G. Kuper, and M.S. Chen, *Microelectron. Reliab.* 38, 1287 (1998).
10. R. Pantaleon, J. Sanchez-Mendoza, and M. Mena, *44th Electronic Components and Technology Conf.* (IEEE Washington, DC, 1994) pp. 733–740.
11. S. Murali, N. Srikanth, and C.J. Vath III, *Microelectron. Reliab.* 46, 467 (2006).
12. T. Saraswati, T. Sritharan, S. Mhaisalkar, C.D. Breach, and F. Wulff, *Mater. Sci. Eng. A.* 423, 14 (2006).
13. M. Shah, K. Zeng, A.A.O. Tay, and S. Suresh, *J. Electron. Packag.* 126, 87 (2002).
14. P.A. Agyakwa, M.R. Corfield, J.F. Li, W. Loh, E. Liotti, S.C. Hogg, and C.M. Johnson, *IEEE Trans. Device Mater. Reliab.* 10, 254 (2010).
15. A. Jalar, M.N. Zulkifli, and S. Abdullah, *Adv. Mater. Res.* 148–149, 1163 (2011).
16. W.C. Oliver and G.M. Pharr, *J. Mater. Res.* 7, 1564 (1992).
17. A.C. Fischer-Cripps, *Introduction to Contact Mechanics* (New York: Springer, 2000), pp. 1–81.
18. S. Murali, N. Srikanth, and C.J. Vath III, *Mater. Charact.* 50, 39 (2003).
19. N. Srikanth, S. Murali, Y.M. Wong, and C.J. Vath III, *Thin Solid Films* 462–463, 339 (2004).
20. T.Y. Zhang and W.H. Xu, *J. Mater. Res.* 17, 1715 (2002).
21. S. Pahak, D. Stojakovic, R. Doherty, and S.R. Kalidindi, *J. Mater. Res.* 24, 1142 (2008).
22. W.D. Nix and H. Gao, *J. Mech. Phys. Solids* 46, 411–425 (1998).
23. R.K.A. Al-Rub, *Mech. Mater.* 39, 787 (2007).
24. G.Z. Voyiadjis and R. Peters, *Acta Mech.* 211, 131 (2010).
25. A.A. Elmustafa and D.S. Stone, *Mater. Lett.* 57, 1072 (2003).
26. K. Durst, B. Backes, and M. Goken, *Scr. Mater.* 52, 1093 (2005).
27. D.R. Askeland and P.P. Pradeep, *The Science and Engineering of Materials* (Toronto: Thomson, 2006), pp. 39–42.
28. Y. Choi and S. Suresh, *Scr. Mater.* 48, 249 (2003).
29. Y. Choi, K.J.V. Vliet, J. Li, and S. Suresh, *J. Appl. Phys.* 94, 6050 (2003).
30. M. Dietiker, R.D. Nyilas, C. Solenthaler, and R. Spolenak, *Acta Mater.* 56, 3887 (2008).
31. J. Lian, J. Wang, Y. Kim, and J. Greer, *J. Mech. Phys. Solids.* 57, 812 (2009).
32. X.H. Wang, S. Jacobsen, J.Y. He, Z.L. Zhang, S.F. Lee, and H.L. Lein, *Cem. Concr. Res.* 39, 701 (2009).
33. A. Daugela, N. Gitis, and V. Gelfeindbein, *Microsyst. Technol.* 16, 33 (2010).
34. A. Bolshakov and G.M. Pharr, *J. Mater. Res.* 13, 1049 (1998).
35. W.C. Oliver and G.M. Pharr, *J. Mater. Res.* 19, 3 (2004).
36. A.C. Fischer-Cripps, *Surf. Coat. Technol.* 200, 4153 (2006).
37. A.C. Fischer-Cripps, *J. Mater. Sci.* 32, 727 (1997).